Journal of Nuclear Science and Technology

ISSN: 0022-3131 (Print) 1881-1248 (Online) Journal homepage: https://www.tandfonline.com/loi/tnst20

A Multicomponent Model of Radiation-induced Segregation for Commercial Stainless Steels

Koji FUKUYA & Katsuhiko FUJII

To cite this article: Koji FUKUYA & Katsuhiko FUJII (2009) A Multicomponent Model of Radiation-induced Segregation for Commercial Stainless Steels, Journal of Nuclear Science and Technology, 46:7, 744-752, DOI: 10.1080/18811248.2007.9711581

To link to this article: https://doi.org/10.1080/18811248.2007.9711581

Published online: 16 Mar 2012.

Journal of NUCLEAR SCIENCE and TECHNOLOGY, Vol. 46, No. 7, p. 744–752 (2009)

ARTICLE

A Multicomponent Model of Radiation-induced Segregation for Commercial Stainless Steels

Koji FUKUYA* and Katsuhiko FUJII

Institute of Nuclear Safety System, 64 Sata, Mihama-cho, Mikata-gun, Fukui 919-1205, Japan

(Received October 27, 2008 and accepted in revised form March 30, 2009)

A radiation-induced segregation model of the Fe-Cr-Ni-Si-Mo system was developed to predict the change in grain boundary composition in commercial stainless steels under neutron irradiation. Parametric survey showed that there were strong influences on segregation behavior for the binding of Si to an interstitial and the jump frequency of Ni and Si via interstitial mechanisms. Careful setting of these parameters using effective point defect migration energies resulted in a good agreement between calculated results and measured data for SUS316 stainless steels irradiated to 74 dpa in light water reactor. Model calculation qualitatively reproduced the effects of dose rate, temperature, and bulk composition reported in the literature.

KEYWORDS: radiation-induced segregation, grain boundary, stainless steels, neutron irradiation, light water reactors, rate theory, vacancy, interstitial

I. Introduction

Radiation-induced segregation (RIS) is known to cause solute redistribution at sinks through point defect flows in various alloy systems.[1–3] In austenitic stainless steels, depletion of Cr and Mo and enrichment of Ni and Si occur at grain boundaries under irradiation. The change in composition of these elements at grain boundaries can alter the electrochemical properties and grain boundary bonding, resulting in the susceptibility of stainless steels to irradiation assisted stress corrosion cracking (IASCC) in light water reactor (LWR) environment.[4–6] It is known that IASCC susceptibility correlates with chemical compositions at grain boundaries. The correlation between the depletion of Cr and IASCC susceptibility in oxygenated water has often been pointed out.[4–6] It is also known that Mo and Si affect IASCC susceptibility. Mo has a beneficial effect of suppressing IASCC susceptibility.[7] The total depletions of Cr and Mo gave a better correlation with IASCC susceptibility than the depletion of Cr alone in 304 and 316 stainless steels.[8] An enhancement effect of Si on IASCC was suggested based on the facts that the susceptibility and propagation of intergranular SCC were higher for higher bulk Si content in unirradiated stainless steels.[9,10] Si has a higher oxidation potential than the other major elements of stainless steels and is supposed to be preferentially oxidized at grain boundaries, becoming a crack path. In commercial stainless steels, Mo is often enriched up to 10 wt% in unirradiated steels at grain boundaries and that Si reaches several wt% in stainless steels irradiated to several dpa, corresponding to a level higher than 10 at%.[8,11,12] Such high concentration of Mo and/or Si is likely to strongly affect RIS of major elements.

Theoretical models of RIS have been developed for stainless steels based on the rate theory approach for the flow of point defects and solute atoms to a grain boundary. For major elements, which are Fe, Cr, and Ni in stainless steels, RIS is attributed to inverse Kirkendall effects, in which slowly diffusing solutes enrich and fast diffusing solutes deplete at sinks via vacancy flux.[13,14] The preferential association of undersized atom with the interstitial flux has been proposed to explain the segregation of major elements.[15] This modeling has been modified and successfully applied to RIS behavior in Fe-Cr-Ni ternary alloys.[16,17] For minor elements such as Si and P, a model of dilute binary alloys has been applied considering the interactions of interstitials and solute atoms.[1,3,19,20] Ternary Fe-Cr-Ni and binary Fe-Si models have been separately used to predict RIS in stainless steels using different physical parameters. RIS in the Fe-Cr-Ni system is known to be suppressed by adding other elements such as interstitial C and N,[21] undersized Si and P,[22] and oversized elements such as Hf and Zr.[23] The effects of additional elements were also modeled by modifying the ternary models. Sakaguchi *et al.* treated Si or P effects by extending four-element models considering the binding of undersized elements and interstitials.[22] The effects of oversized elements were modeled by considering the trapping of point defects by the oversized atoms.[24,25] Although RIS of the undersized or oversized element itself was not calculated in these studies, their results implied that the redistribution of undersized and oversized atoms due to RIS has strong effects on RIS of major elements. As mentioned above,

*Corresponding author, E-mail: fukuya@inss.co.jp

current modeling works of RIS in stainless steels do not include the influences of Si and Mo, which likely affect IASCC susceptibility.

In the present study, an RIS model for the Fe-Cr-Ni-Mo-Si multicomponent alloy system was developed to predict RIS in commercial SUS316 stainless steel under irradiation conditions in light water reactors by adjusting physical parameters to fit the measurement data of grain boundary compositions.

II. Calculation Model

1. Model Equations

One approach for modeling of multicomponent RIS is to consider the interactions of each solute with other solutes and point defects and their mobility. Recently, the importance of migration of vacancy-solute complex has been pointed out.[26] However, such an approach requires knowledge of the interaction energy and migration energy of all possible combinations of solutes and point defects, most of which are still unknown. Thus, in the present model, it is assumed that the flux of a solute is determined by its effective partial diffusion via vacancy and interstitial mechanisms, extending the Fe-Cr-Ni ternary model proposed by Lam *et al.*[15] to a five-element system. Rate equations for point defects and solutes are

$$\frac{\partial C_{v,i}}{\partial t} = -\nabla J_{v,i} + G_{v,i} - R_{v,i} - S_{v,i}, \tag{1-1}$$

$$\frac{\partial C_k}{\partial t} = -\nabla J_k \quad (k = \text{Fe, Cr, Ni, Mo, Si}), \tag{1-2}$$

where C is the concentration, J is the flux of each species, and $G_{v,i}$, $R_{v,i}$, and $S_{v,i}$ are production rate, recombination rate, and sink absorption rate of point defects, respectively. The fluxes of vacancies (J_v), interstitials (J_i), and solutes (J_k) are

$$J_v = -D_v \nabla C_v + C_v \sum_k d_k^v \nabla C_k, \tag{2-1}$$

$$J_i = -D_i \nabla C_i - C_i \sum_k d_k^i \nabla C_k, \tag{2-2}$$

$$J_k = -D_k \nabla C_k + C_k (d_k^v \nabla C_v - d_k^i \beta_k \nabla C_i). \tag{2-3}$$

The diffusivities of point defects ($D_{v,i}$) and solutes (D_k) are given by using partial diffusion coefficients ($d_k^{v,i}$):

$$D_v = \sum_k d_k^v C_k, \tag{3-1}$$

$$D_i = \sum_k d_k^i \beta_k C_k, \tag{3-2}$$

$$D_k = d_k^v C_v + d_k^i \beta_k C_i. \tag{3-3}$$

The partial diffusion coefficients of solute k by the vacancy or interstitial mechanism are determined as

$$d_k^{v,i} = \nu_{v,i} \omega_{k-v,i} {a_0}^2 \exp\left(-\frac{E_{k-v,i}^m}{kT}\right), \tag{4}$$

where $\nu_{v,i}$ is the jump frequency of the vacancy and interstitial atom via the k-atom, $\varpi_{v,i}$ is the relative jump frequency factors to the Fe atom, a_0 is the lattice constant, and $E_{k-v,i}^m$ is the migration energy of the vacancy or interstitial. The coupling parameter β_k provides the fraction of each solute forming the mixed dumbbell and is described as

$$\beta_k = \frac{\exp(E_{k-i}^b/kT)}{\sum_k C_k \exp(E_{k-i}^b/kT)}, \tag{5}$$

where E_{k-i}^b is the binding energy between an interstitial and solute atom.

The production rate and recombination rate of point defects are expressed as $G_{v,i} = \eta G_{dpa}$ and $R_{v,i} = RD_i C_v C_i$, respectively, where η is the defect production efficiency, G_{dpa} is the displacement per atom (dpa) rate, and R is the recombination volute. The sink annihilation rate is expressed as $S_v = \rho Z_v D_v (C_v - C_v^e)$ and $S_i = \rho Z_i D_i C_i$, where ρ is the sink density, $Z_{v,i}$ is the sink bias for point defects, and C_v^e is the thermal equilibrium vacancy concentration. The boundary conditions at time t were set $J_k(L,t) = 0$ and $J_{v,i}(L,t) = 0$ at the center of the grain where L is the distance from the grain boundary, $J_k(0,t) = 0$ and $C_{v,i}(0,t) = C_{v,i}^e$ at the grain boundary where $C_{v,i}^e$ is the thermal equilibrium concentration of vacancy and interstitial. In the present model, the distribution of secondary defects near grain boundaries is ignored for simplicity, the same as in previous modeling works.

2. Material Parameters

Most of the material parameters for vacancies, interstitials, and Fe, Cr, and Ni were selected to be consistent with those used in Fe-Cr-Ni ternary models, whereas some modifications were necessary to fit the model calculation to RIS data in commercial stainless steels. The previous studies showed that RIS in stainless steels depended on the amount of other minor elements such as C, N, and P, and that a higher amount of these elements resulted in a lower RIS.[21,27] This is likely due to lower effective mobility of vacancies and interstitials in steels containing higher levels of impurities that trap point defects. The migration energies of vacancies and interstitials were expected to be higher than the often-used values of 1.3 and 0.9 eV[16,17] and were assumed to be 1.4–1.5 eV and 1.0–1.1 eV, respectively.

The difference in the partial diffusion coefficients of each solute by the vacancy mechanism, d_k^v, which is the driving force of inverse Kirkendale effects, is considered as the difference in the relative jump frequency factor ω_{k-v}. The migration energy is assumed to be the same for all five elements. The literature data showed that the diffusion coefficients of Si and Mo are almost one order of magnitude higher than that of Fe in austenitic iron- or nickel-based alloys.[28,29] However, trial calculation revealed that such high values resulted in excess depletion of Mo and Si. Thus, the adjustment was made in the range of relative jump frequency factor ω_{k-v} of 2–5 for both Si and Mo. In the present model, a higher Si diffusion coefficient increases the vacancy diffusion, which is consistent with the fact that adding Si increases the effective vacancy diffusion.[30]

The partial diffusion coefficients of each solute by the interstitial mechanism and the binding energy between an interstitial atom and solute atom are selected as follows. Binding with interstitials is assumed for Si alone. Previous

studies examining the effect of P or Si addition on interstitial loop nucleation using electron irradiation suggested that Si has a smaller binding energy with interstitials than P.[31] Watanabe *et al.* showed that the effective binding energy of P with interstitials is 0.5 eV in Fe-Cr-Ni alloys.[32] Thus, in this study, the binding energy between a Si atom and an interstitial is assumed to be 0.1–0.3 eV. A similar value was reported by Simonen *et al.* for modeling of RIS of Si in stainless steels.[33]

The influence of alloy composition on RIS was considered as follows. In previous experimental studies, the suppression effect of Si[24] and enhancement effect of Ni[16,34] on RIS were reported, whereas there was no clear evidence that Cr and Mo affect RIS.[34] To include compositional effects in the RIS model in the Fe-Cr-Ni ternary system, Perks *et al.* adopted the composition-dependent migration energies of vacancies and interstitials proposed by Dimitrov *et al.*[14,35] Allen and Was considered the composition-dependent diffusivity and short-range ordering force in the vacancy mechanism.[36] These models assumed that the partial diffusion coefficients of Fe, Cr, and Ni atoms by the interstitial mechanism were identical. It would have been difficult to adopt a similar approach in the present model since the effects of Si and Mo on diffusivity were not known. Thus, no compositional effect was assumed for the migration energy, whereas the different partial diffusion coefficient of each solute was assumed by changing the relative jump frequency factor ω_{k-i}. In the previous binary Fe-Si models, it was assumed that two types of Si-interstitial complex exist, mobile and immobile, and that the mobile Si-interstitial complex has a high migration energy of 1.4–1.8 eV. These assumptions resulted in a lower effective mobility of Si atoms via the interstitial mechanism than that of Fe atoms. To maintain consistency with the previous models, a lower relative jump frequency factor for Si than for Fe was assumed in this study. However, the combination of Si-interstitial binding energy and relative jump frequency factor for Si ($\omega_{Si\text{-}i}$) needed to be carefully selected, since the combination of higher binding energy and lower $\omega_{Si\text{-}i}$ resulted in a lower net mobility of interstitials in Eq. (3-2) than the net mobility of vacancies in Eq. (3-1). A higher relative jump frequency factor for Ni than that for Fe was assumed so as to correlate with the reported enhancement effects of Ni on RIS[34] and with a higher interstitial mobility with increasing Ni concentration in Fe-Cr-Ni ternary alloys.[35]

III. Results and Discussion

First, to check the relative influence of each parameter, calculations were performed by changing the parameter values for typical 316 stainless steel (Fe-17Cr-13Ni-0.5Si-2.5Mo in wt%) in typical LWR conditions (573 K, 1×10^{-7} dpa/s). Other constants were assumed to be 3×10^{14} m^{-2} for dislocation density, 1.6 eV for vacancy formation energy, and 1.1 for dislocation sink bias for interstitials. **Table 1** shows the range of values and their relative influence on RIS. In this procedure, calculations were performed by changing one parameter while also changing other parameters. Among a large number of combinations of parameters, significant influences on RIS were observed for the relative jump frequency factor of solute-interstitial complex and solute-vacancy complex for Ni and Si, and the binding energy between Si and interstitial. **Figure 1** shows examples of such influences for relative jump frequency factor of Ni via interstitial and interstitial-Si binding energy. An increase in relative jump frequency for Ni via interstitial resulted in an increase in Ni segregation without notable changes in other solutes. An increase in Si-interstitial binding energy caused an increase in the fraction of interstitial flux coupled with Si and in turn a decrease in interstitial flux coupled with Ni, resulting in a strong decrease in Ni enrichment. A higher Si-interstitial binding energy, 0.25 eV, resulted in unrealistic behavior such that the Ni enrichment decreased with increasing dose and became lower than Si, probably due to a higher back diffusion rate than low Ni segregation via interstitial mechanism.

Table 1 Range of assumed parameters

Parameter		Range of value	Relative influence on RIS
Vacancy migration energy		1.3–1.5	weak
Relative jump frequency factor via vacancy ϖ_{k-v}	Fe	1	—
	Cr	1.1–1.3	weak
	Ni	0.4–0.6	strong
	Si	3–7	medium
	Mo	2–6	weak
Interstitial migration energy		0.9–1.1	
Relative jump frequency factor via interstitial ϖ_{k-i}	Fe	1	—
	Cr	1	—
	Ni	1.2–1.6	strong
	Si	0.3–0.7	strong
	Mo	1	—
Interstitial-solute binding energy (eV)	Si	0.15–0.25	strong

The final determination of parameters was carried out by fitting to measured data, which were obtained in cold-worked SUS316 stainless steels irradiated as flux thimble tubes in a pressurized water reactor.[12] The irradiation conditions were 565–596 K for temperature, 1–73 dpa for dose, and 3×10^{-9}–1.5×10^{-7} dpa/s for dose rate. The measurements were performed across three high-angle grain boundaries for each condition by using energy-dispersive X-ray analysis with a probe beam diameter of 2 nm. The calculation results were converted to corrected values corresponding to measurement condition by using the following equation:

$$C'(X) = \frac{\int c(x) \exp\{-(x-X)^2/2R^2\} dx}{\int \exp\{-(x-X)^2/2R^2\} dx}. \quad (6)$$

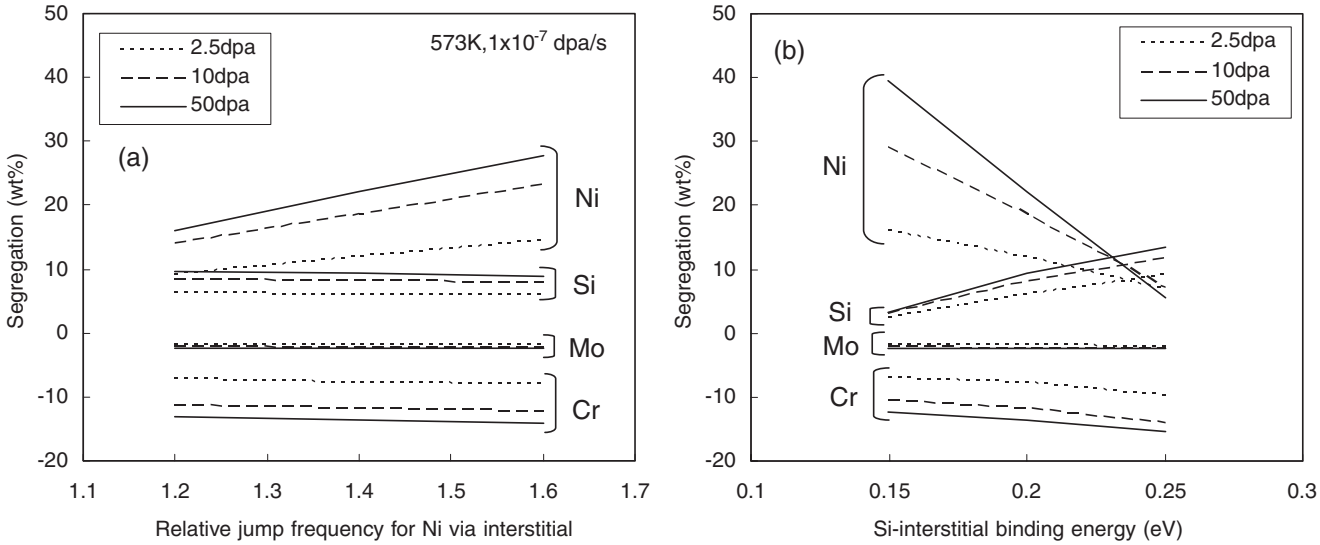

Fig. 1 Influence of (a) relative jump frequency factor of Ni via interstitial and (b) interstitial-Si binding energy on RIS

$C'(X)$ is the corrected concentration of solutes, $c(x)$ is the calculated concentration, x or X is the normal distance from the grain boundary, and R ($\sim$1 nm) is the variance of the probe beam assuming that the beam intensity has a Gaussian distribution. The range of the integration was taken to be a sufficiently larger distance than R. For pre-irradiation segregation, a normalized function of concentration distribution across the grain boundary was composed so that the measured distribution was reproduced by using the normalized function and Eq. (6).

Table 2 summarizes the determined parameters, together with parameter sets in other models.[22,37] The difference in parameter sets among models is likely attributed to the difference in data fitted to model calculations. Sakaguchi *et al.* and Allen *et al.* applied their models to data of pure Fe-Cr-Ni alloys under electron and proton irradiation at low doses.[22,37] **Figure 2** compares solute distributions for calculated and measured data for lower flux and higher flux. In this figure, each calculation was conducted under dose rate and temperature conditions in the table and plotted with a line terminated at the dose of each data. **Figure 3** compares segregation at the grain boundary between calculated results and measured data as a function of dose. **Figure 4** shows plots of measured versus calculated segregation at grain boundaries. Segregation is defined as a difference in concentration between grain boundary and bulk in these figures. The distribution, dose dependence, and segregation levels calculated in the present model with the determined parameters were in good agreement with those measured for all elements. It was thus demonstrated that the present model and determined parameters offer excellent prediction capability of grain boundary segregation in the referred data.

The parameters were determined by fitting to a single data set of cold-worked SUS316 stainless steels with narrow ranges of temperature and dose rate. Thus, the applicability of the present model and parameters to wider ranges of irradiation condition and material composition was qualitatively examined by comparing the calculated results with the influences reported in the literature. The calculations were

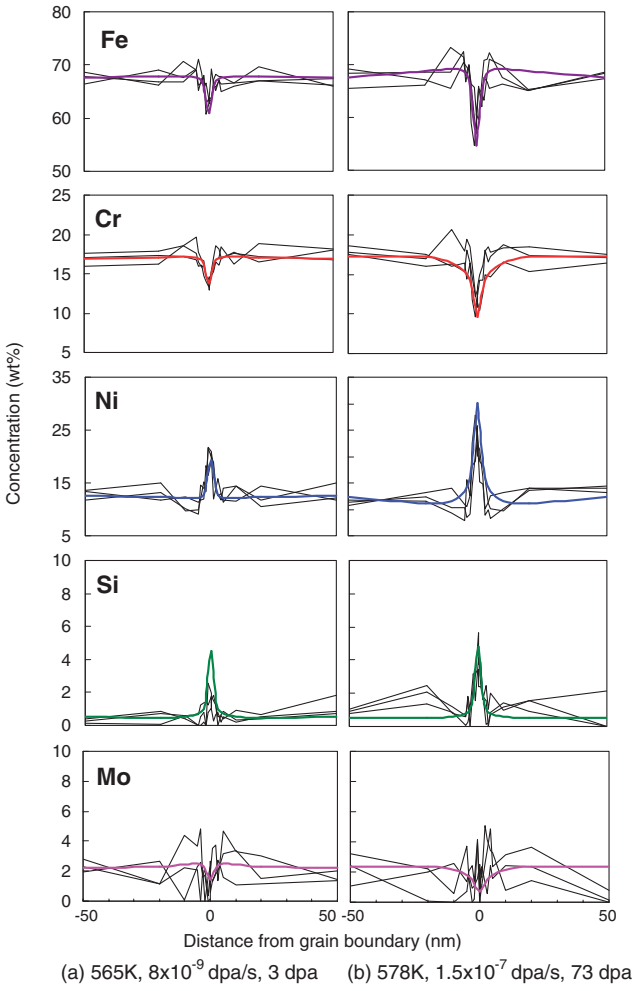

Fig. 2 Comparison of solute distribution near grain boundary between measurements (thin lines) and calculations (thick colored lines)

carried out while changing the irradiation and material parameters for a standard condition: temperature of 573 K, dose rate of 1×10^{-7} dpa/s, and dislocation density of

Table 2 Summary of parameters used in the model

Parameter			This work Fe-Cr-Ni-Si-Mo	Sakaguchi[22] Fe-Cr-Ni-Si	Allen[37] Fe-Cr-Ni
Vacancy	Jump frequency ν_v(/s)		1.5×10^{12}	5×10^{13}	1.5×10^{13}
	Relative jump frequency ω_{k-v}	Fe	1	1	1
		Cr	1.1	1.6	1.785
		Ni	0.4	0.5	0.3
		Si	3	10	—
		Mo	1.5	—	—
	Migration energy E^m_{k-v}(eV)	Fe	1.5	1.05	1.3
		Cr	1.5	1.05	1.3
		Ni	1.5	1.05	1.3
		Si	1.5	1.05	—
		Mo	1.5	—	—
	Formation energy E^f_v(eV)		1.6	1.6	1.9
	Formation enthalpy S^f_v		1.5	1.5	1
Interstitial	Jump frequency ν_i(/s)		1.5×10^{12}	5×10^{12}	1.5×10^{12}
	Relative jump frequency ω_{k-i}	Fe	1	1	1
		Cr	1	1	1
		Ni	1.3	1	1
		Si	0.5	1	—
		Mo	1	—	—
	Migration energy E^m_{k-i}(eV)	Fe	1.1	0.85	0.9
		Cr	1.1	0.85	0.9
		Ni	1.1	0.85	0.9
		Si	1.1	1.4	—
		Mo	1.1	—	—
	Binding energy E^b_{k-i}(eV)	Fe	0	0	0
		Cr	0	0	0
		Ni	0	0.75	0
		Si	0.2	0.7	—
		Mo	0	—	—
	Dislocation bias Z^d_i		1.1	1.25	—
Damage efficiency η			0.03	—	0.02
Recombination volume Z_{v-i}			500	—	12

$3 \times 10^{14}/m^2$ for the composition of Fe-17Cr-13Ni-0.5Si-2.5Mo in wt%. In the calculations, the measurement beam correction shown in Eq. (6) was included. Since it is well known that temperature and dose rate affect microstructure evolution and then sink strength to point defects, the influence of sink strength on RIS was examined at 573 and 773 K as shown in **Fig. 5**. The sink density was changed by changing the dislocation density from 10^{10} to $10^{15}/m^2$, considering the case of a smaller contribution of cavity than that of dislocations. The influence of sink density appeared at above $10^{14}/m^2$ at 773 K, while it was negligible in the entire range at 573 K and at lower dislocation density at 773 K. It is also known that the dislocation density increases with dose and saturates at 10–20 dpa, and that the saturated dislocation density including Frank loops and perfect loops at 373–923 K ranged from 10^{14} to $10^{15}/m^2$ and became lower for higher temperature in type 316 stainless steels.[38] Thus, model calculation using dislocation density of $3 \times 10^{14}/m^2$ is expected to give us the general features of temperature and dose rate dependence of RIS. **Figure 6** shows model calculations for the temperature dependence of segregation for different dose rates of 10^{-9}–10^{-3} dpa/s at 10 dpa. Ni, Cr, and Mo showed almost the same peak temperature, which became lower for lower dose rate. For a fixed temperature, the segregation became lower for higher dose rate at temperatures below the peak. These influences of temperature and dose rate coincided with the previous model calculation for Fe-Cr-Ni ternary systems. Si showed a lower peak temperature than the other solutes. The peak temperature of Si was about 100 K lower than that of the other solutes. The Si concentration at the peak temperature increased with decreasing dose rate.

Although systematic RIS data of commercial 316 stainless steels with changing temperature and dose rate are scarce in the literature, the calculated results were qualitatively comparable to the experimental data in the literature. As for

Irradiation condition of each data and model calculation

Dose (dpa)	0	3	11	25	31	35	38	53	73
Temperature (C)	-	566	596	596	567	586	571	577	578
Dose rate (dpa/s)	-	$8x10^{-9}$	$3x10^{-8}$	$6x10^{-8}$	$8x10^{-8}$	$1.3x10^{-7}$	$8x10^{-8}$	$1.4x10^{-7}$	$1.5x10^{-7}$

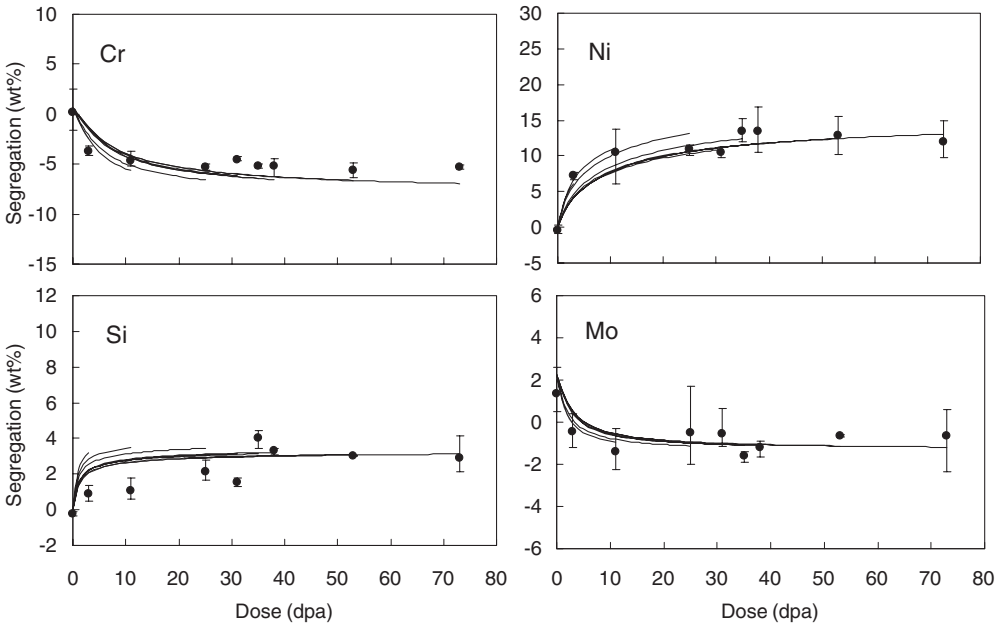

Fig. 3 Comparison of RIS between measurements (closed circles) and calculation results (solid lines) as a function of dose in CW316 stainless steels

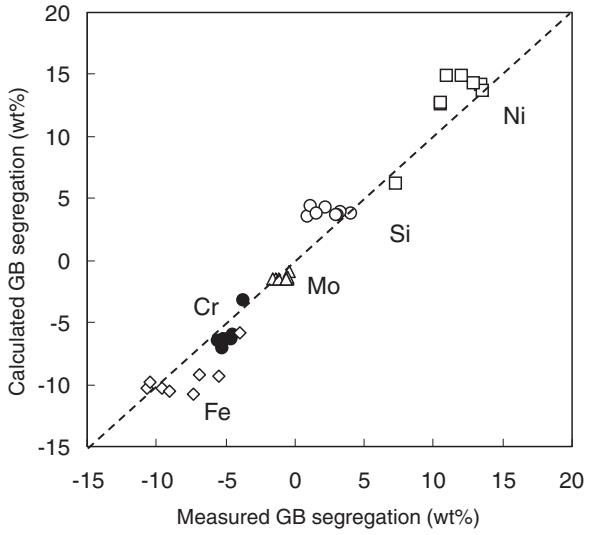

Fig. 4 Plot of measured versus calculated RIS in CW316 stainless steels

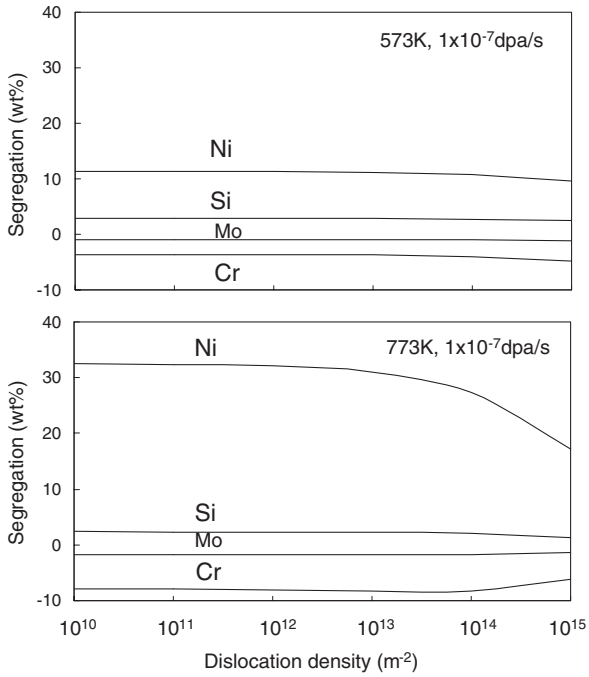

Fig. 5 Effect of dislocation density on RIS at 10 dpa

high-dose-rate irradiation, Nakata and Masaoka reported RIS behavior in 316 L stainless steels at temperatures from 673 to 873 K under electron irradiation at a dose rate of 2.7×10^{-3} dpa/s.[39] They found that the peak RIS occurred at 773 K for Si and at above 873 K for Cr, Ni, and Mo. Their results agree well with the present calculation results. In the low-dose-rate region of 10^{-8} to 10^{-6} dpa/s relevant to reactor irradiation, LWR data were reported at temperatures of 560–623 K at a dose rate of 10^{-8}–10^{-7} dpa/s.[8,11,12,40,41] At doses of 10–20 dpa, Cr depletion and Ni enrichment were 4–7 wt% and 10–14 wt%, respectively. Fast breeder reactor (FBR) data were also reported at a temperature of 593–653 K at a dose rate of 10^{-7}–10^{-6} dpa/s.[40,43–45] At doses of 10–20 dpa, Cr depletion and Ni enrichment were 2–3 wt% and 3–10 wt%, respectively. The model calculation predicted 6 and 12 wt% for Cr depletion and Ni enrichment, respectively, at a dose rate of 10^{-8} dpa/s at 573 K, and 3 and

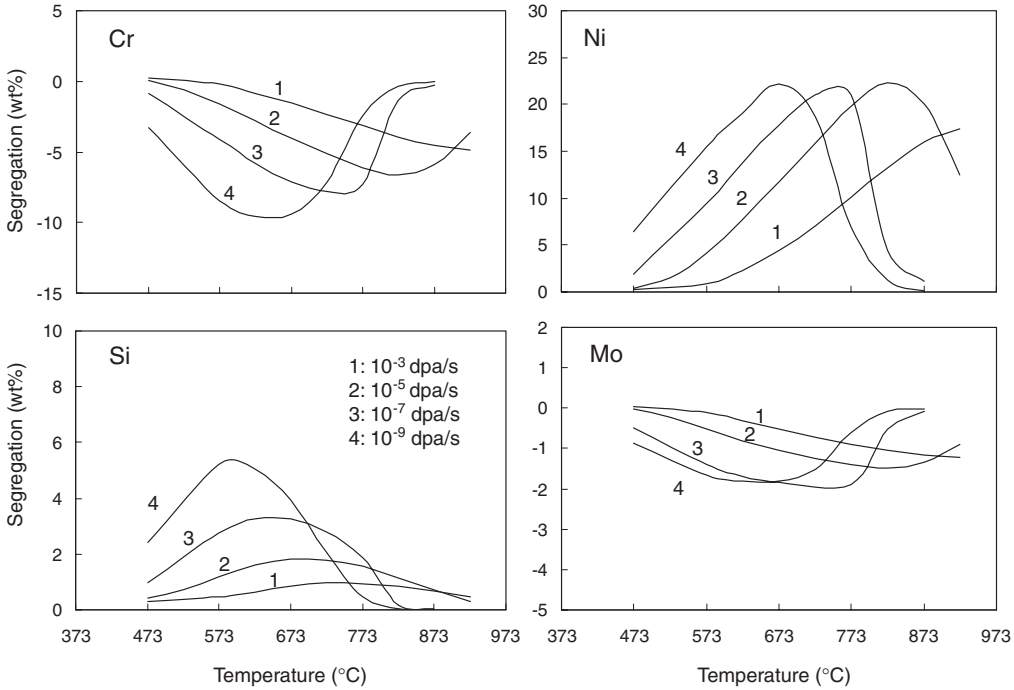

Fig. 6 Effect of temperature and dose rate on RIS at 10 dpa

7 wt%, respectively, at a dose rate of 10^{-6} dpa/s at 623 K. Considering that a large scatter existed in the database due to the difference in composition, probe quality in analysis, initial segregation level, and so on, the model provided reasonable prediction in the above dose rate and temperature conditions.

As for Si and Mo, the experimental values in the literature were 1–5 wt% for Si and 0.5–1.7 wt% for Mo at 10–20 dpa. The differences in segregation between FBR and LWR irradiation were not clear. The model predicted similar values. The present model predicted that the peak temperature of Si segregation was lower than that in other elements. This is because Si is transported to grain boundaries as a complex with an interstitial, whereas the segregation of other solutes is determined mainly by vacancy mechanism in the present model. As the temperature increases, the dissociation probability of the complex increases, whereas the flux of the complex to grain boundaries decreases. The peak temperature of Si segregation was 773 K at a dose rate of 10^{-3} dpa/s from the model prediction and was consistent with the experimental results as mentioned above. The model predicts that the peak temperature decreases to 573 K at a dose rate of 1×10^{-9} dpa/s. On the other hand, Simonen *et al.* predicted a very low peak temperature, 373 K, at 2×10^{-8} dpa/s using the Fe-Si binary model with interstitial-solute binding energy of 0.2 eV.[33] Lack of data on temperature dependence of Si segregation at the low-dose-rate region made it difficult to discuss this further at this moment. Systematic data are needed to confirm the effects of dose rate and temperature on RIS of Si.

Figure 7 shows model calculations for the effects of bulk composition of Cr, Ni, Si, and Mo on segregation at 573 K at a dose rate of 10^{-7} dpa/s. An increase in bulk Cr concentration enhanced Cr depletion but caused no changes in other elements. An increase in bulk Ni concentration caused larger Ni enrichment and Cr depletion and smaller Si enrichment. The behaviors of the major elements, Cr and Ni, in the present calculation were qualitatively consistent with predictions using previous Fe-Cr-Ni ternary models[18,37] and experimental results of Fe-Cr-Ni ternary alloys under proton and electron irradiation at 673 K.[34,46] A higher bulk Si concentration caused smaller Ni enrichment and slightly larger Cr depletion at high doses together with larger Si enrichment. Such effects of Si on Cr and Ni segregation were larger at lower temperatures. Sakaguchi *et al.* found strong suppression effects on Ni enrichment and weak suppression effects on Cr depletion in their electron irradiation experiment for solution-treated Fe-15Cr-20Ni-0.5Si alloy under electron irradiation to 1.8 dpa at 573 K at a dose rate of 1×10^{-3} dpa/s and in calculations using their Fe-Cr-Ni-Si model.[24] In the present calculation under a condition corresponding to their calculation, Si addition had small suppression effects on Ni enrichment and almost no effect on Cr depletion. A smaller assumed Si-interstitial binding energy of 0.2 eV than their value of 0.7 eV is likely to result in a smaller fraction of Si-interstitial complex in the net interstitial flow to grain boundaries and thus weak effects of Si on the segregation of the major elements. The bulk concentration of Mo had no effects on the segregation of the elements other than Mo itself, which showed a higher depletion for higher bulk Mo concentration. This result was consistent with experimental data of Fe-16Cr-13Ni-Mo alloys at 673 K at a dose rate of 7×10^{-6} dpa/s.[34]

As mentioned above, the present model and parameters can qualitatively reproduce general RIS behavior and influences of irradiation conditions and material compositions. Systematic neutron irradiation data is needed for quantitative calculations under LWR conditions.

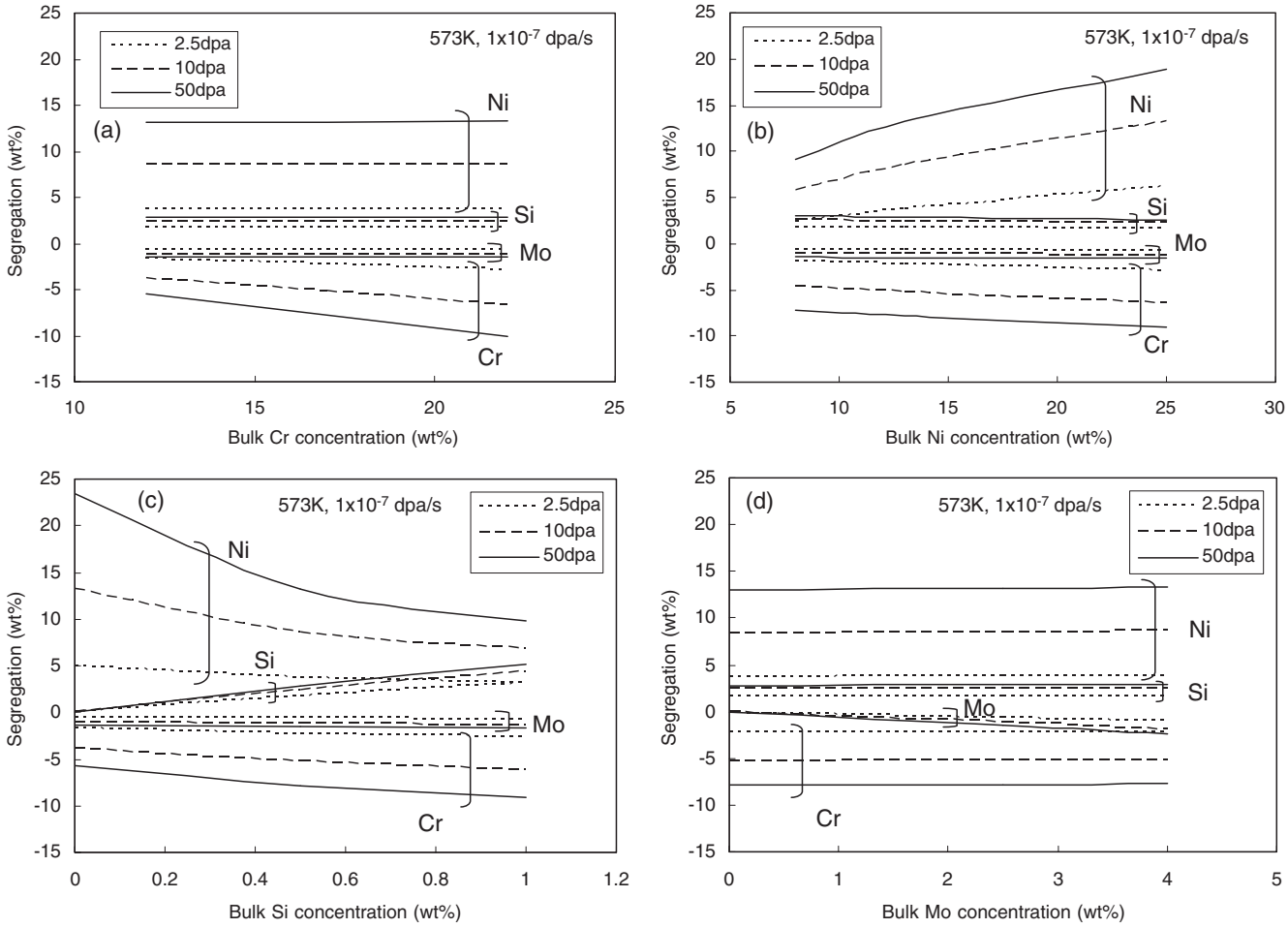

Fig. 7 Effect of bulk composition of (a) Cr, (b) Ni, (c) Si, and (d) Mo on RIS at 573 K

IV. Conclusions

A radiation-induced segregation model for the Fe-Cr-Ni-Si-Mo multicomponent alloy system was applied to grain boundary segregation in commercial stainless steels under irradiation conditions relevant to light water reactors. Physical parameters in the model were determined to fit measured data in highly irradiated SUS316 stainless steels. The results of calculations using the model with the determined parameters were qualitatively consistent with the known effects of temperature, dose rate, and material compositions.

References

1) P. R. Okamoto, L. E. Rehn, *J. Nucl. Mater.*, **83**, 2 (1979).
2) A. D. Marwick, *J. Phys. F*, **8**, 1849 (1978).
3) R. A. Johnson, N. Q. Lam, *Phys. Review B*, **13**, 4364 (1976).
4) G. S. Was, S. M. Bruemmer, *J. Nucl. Mater.*, **216**, 326 (1994).
5) P. Scott, *J. Nucl. Mater.*, **211**, 101 (1994).
6) H. M. Chung, W. E. Ruther, J. E. Sanecki *et al.*, *J. Nucl. Mater.*, **239**, 61 (1996).
7) A. Jenssen, L. G. Ljungberg, J. Walmsley, S. Fisher, *Corrosion 96*, paper No. 101, NACE (1996).
8) M. Kodama, Y. Ishiyama, S. Namatame, S. Suzuki, K. Fukuya, H. Sakamoto, K. Nakata, T. Kato, *Proc. 9th Int. Symp. on Environmental Degradation of Materials in Nuclear Power Systems—Water Reactors*, TMS, 923 (1991).
9) P. L. Andresen, P. W. Emith, M. M. Morra, R. M. Horn, *Proc. 11th Int. Symp. on Environmental Degradation of Materials in Nuclear Power Systems—Water Reactors*, ANS (1991).
10) G. F. Li, Y. Kaneshima, T. Shoji, *Corrosion*, **56**, 460 (2000).
11) K. Asano, K. Fukuya, K. Nakata, M. Kodama, *Proc. 5th Int. Symp. on Environmental Degradation of Materials in Nuclear Power Systems—Water Reactors*, ANS, 838 (1991).
12) K. Fukuya, K. Fujii, M. Nishioka, Y. Kitsunai, *J. Nucl. Sci. Technol.*, **43**, 159 (2006).
13) A. D. Marwick *et al.*, *Dimensional Stability and Mechanical Behavior of Irradiated Metals*, British Nuclear Energy Society, London, 11 (1984).
14) J. M. Perks *et al.*, *Materials for Nuclear Reactor Core Applications*, Nuclear Energy Society, London, 165 (1987).
15) N. Q. Lam, A. Kumar, H. Wiedersich, *Effects of Radiation on Materials: Eleventh Conf.*, ASTM STP 782, 985 (1982).
16) T. R. Allen, G. S. Was, E. A. Kenik, *J. Nucl. Mater.*, **224**, 278 (1997).
17) E. P. Simonen, S. M. Bruemmer, *J. Nucl. Mater.*, **239**, 185 (1996).
18) S. Watanabe, N. Sakaguchi, N. Hashimoto, H. Takahashi, *J. Nucl. Mater.*, **224**, 158 (1995).
19) S. M. Murphy, *J. Nucl. Mater.*, **168**, 31 (1989).
20) T. Hashimoto, Y. Isobe, N. Shigenaka, *J. Nucl. Mater.*, **225**, 108 (1995).
21) F. Kano, K. Fukuya, S. Hamada, Y. Miwa, *J. Nucl. Mater.*,

258–263, 1713 (1998).
22) N. Sakaguchi, H. Takahashi, H. Ichinose, *Materials Trans.*, **46**, 440 (2005).
23) T. Kato, H. Takahashi, M. Izumiya, *Mater. Trans. JIM*, **32**, 921 (1991).
24) N. Sakaguchi, S. Watanabe, H. Takahashi, *Nucl. Instrum. Methods Phys. Res.*, **B153**, 142 (1999).
25) M. J. Hackett, G. S. Was, E. P. Simonen, *J. ASTM Int.*, **2**, JAI12406 (2005).
26) J. D. Tucker, T. R. Allen, D. Morgan, *Proc. 13th Int. Conf. on Environmental Degradation of Materials in Nuclear Power Systems—Water Reactors*, CNS (2007).
27) A. J. Jacobs *et al.*, *Corrosion 94*, paper No. 124, NACE (1994).
28) Y. Iijima, K. Hirano, *Diffusion Processes in Nuclear Materials*, Elsevier (1992).
29) P. J. Maziasz *et al.*, *Mater. Review*, **12**, 190 (1987).
30) B. Esmailzadeh, A. Kumar, F. A. Garner, *J. Nucl. Mater.*, **133–134**, 590 (1985).
31) K. Fukuya, S. Nakahigashi, S. Ozaki, M. Terasawa, S. Shima, *Proc. 3rd Int. Symp. on Environmental Degradation of Materials in Nuclear Power Systems—Water Reactors*, TMS, 665 (1987).
32) H. Watanabe, A. Aoki, H. Murakami *et al.*, *J. Nucl. Mater.*, **155–157**, 815 (1988).
33) E. P. Simonen, D. J. Edwards, S. M. Brummer, *Proc. 12th Int. Conf. on Environmental Degradation of Materials in Nuclear Power Systems—Water Reactors*, TMS, 429 (2005).
34) J. I. Cole, T. R. Allen, G. S. Was, Y. Wang, E. A. Kenik, *Proc. 10th Int. Conf. on Environmental Degradation of Materials in Nuclear Power Systems—Water Reactors*, NACE (2005).
35) C. Dimitrov *et al.*, *Materials Science Forum*, **15–19**, 1275 (1987).
36) T. R. Allen, G. S. Was, *Acta Mater.*, **46**, 3679 (1998).
37) T. R. Allen, J. T. Busby, G. S. Was, E. A. Kenik, *J. Nucl. Mater.*, **255**, 44 (1998).
38) S. J. Zinkle, P. J. Maziasz, R. E. Stoller, *J. Nucl. Mater.*, **206**, 266 (1993).
39) K. Nakata, I. Masaoka, *J. Nucl. Mater.*, **150**, 186 (1987).
40) K. Fujimoto, T. Yonezawa, E. Wachi *et al.*, *Proc. 12th Int. Conf. on Environmental Degradation of Materials in Nuclear Power Systems—Water Reactors*, TMS, 299 (2005).
41) K. Chatani, Y. Kitsunai, M. Kodama *et al.*, *Proc. 12th Int. Conf. on Environmental Degradation of Materials in Nuclear Power Systems—Water Reactors*, TMS, 349 (2005).
42) D. J. Edwards, E. P. Simonen, F. A. Garner *et al.*, *J. Nucl. Mater.*, **317**, 32 (2003).
43) D. J. Edwards, E. P. Simonen, S. M. Bruemmer, *Proc. 13th Int. Conf. on Environmental Degradation of Materials in Nuclear Power Systems—Water Reactors*, CNS (2007).
44) T. R. Allen, J. I. Cole, C. L. Trybus *et al.*, *J. Nucl. Mater.*, **348**, 148 (2006).
45) T. R. Allen, J. I. Cole, J. Ohta *et al.*, *Mat. Res. Soc. Symp. Proc.*, **650** (2001).
46) S. Watanabe, H. Kinoshita, N. Sakaguchi, H. Takahashi, *J. Nucl. Mater.*, **226**, 330 (1995).